NIH Public Access
Author Manuscript
Clin Cancer Res. Author manuscript; available in PMC 2015 May 01.

Published in final edited form as:
Clin Cancer Res. 2014 May 1; 20(9): 2350–2362. doi:10.1158/1078-0432.CCR-13-3033.

Increased KIT inhibition enhances therapeutic efficacy in gastrointestinal stromal tumor

Teresa S. Kim[1], **Michael J. Cavnar**[1], **Noah A. Cohen**[1], **Eric C. Sorenson**[1], **Jonathan B. Greer**[1], **Adrian M. Seifert**[1], **Megan H. Crawley**[1], **Benjamin L. Green**[1], **Rachel Popow**[1], **Nagavarakishore Pillarsetty**[2], **Darren R. Veach**[2], **Anson T. Ku**[2], **Ferdinand Rossi**[1,3], **Peter Besmer**[3], **Cristina R. Antonescu**[4], **Shan Zeng**[1], and **Ronald P. DeMatteo**[1]

[1]Department of Surgery, Memorial Sloan-Kettering Cancer Center, New York, NY

[2]Department of Radiology, Memorial Sloan-Kettering Cancer Center, New York, NY

[3]Department of Developmental Biology, Memorial Sloan-Kettering Cancer Center, New York, NY

[4]Department of Pathology, Memorial Sloan-Kettering Cancer Center, New York, NY

Abstract

Purpose—Gastrointestinal stromal tumor (GIST) is the most common human sarcoma and a model of targeted molecular therapy. GIST depends on oncogenic KIT signaling and responds to the tyrosine kinase inhibitor imatinib. However, imatinib is rarely curative. We hypothesized that PLX3397, which inhibits KIT and CSF1R, would be more efficacious than imatinib in GIST by also depleting tumor-associated macrophages, which are generally thought to support tumor growth.

Experimental Design—We treated *Kit*$^{V558del/+}$ mice that develop GIST or mice with subcutaneous human GIST xenografts with imatinib or PLX3397 and analyzed tumor weight, cellular composition, histology, molecular signaling, and fibrosis. In vitro assays on human GIST cell lines were also performed.

Results—PLX3397 was more effective than imatinib in reducing tumor weight and cellularity in both *Kit*$^{V558del/+}$ murine GIST and human GIST xenografts. The superiority of PLX3397 did not depend on depletion of tumor-associated macrophages, since adding CSF1R inhibition did not

Corresponding author: Ronald P. DeMatteo, MD, Memorial Sloan-Kettering Cancer Center, 1275 York Avenue, New York, NY 10065, Tel: (212) 639-3976, Fax: (212) 639-4031, dematter@mskcc.org.

Disclosure of Potential Conflicts of Interest: R.P.D. has previously served as a consultant for Novartis.

Author Contributions:
Conception and design: T.S. Kim, M.J. Cavnar, E.C. Sorenson, J.B. Greer, N.A. Cohen, A.M. Seifert, N. Pillarsetty, D.R. Veach, A.T. Ku, S. Zeng, R.P. DeMatteo
Development of methodology: T.S. Kim, M.J. Cavnar, S. Zeng, R.P. DeMatteo
Acquisition of data: T.S. Kim, M.J. Cavnar, S. Zeng, N.A. Cohen, M.H. Crawley, B.L. Green, R. Popow, N. Pillarsetty, D.R. Veach, A.T. Ku
Analysis and interpretation of data: T.S. Kim, M.J. Cavnar, E.C. Sorenson, J.B. Greer, N.A. Cohen, A.M. Seifert, M.H. Crawley, B.L. Green, R. Popow, N. Pillarsetty, D.R. Veach, A.T. Ku, F. Rossi, P. Besmer, C.R. Antonescu, S. Zeng, R.P. DeMatteo
Writing, review and/or revision of the manuscript: T.S. Kim, M.J. Cavnar, E.C. Sorenson, J.B. Greer, N.A. Cohen, A.M. Seifert, M.H. Crawley, B.L. Green, R. Popow, N. Pillarsetty, D.R. Veach, A.T. Ku, F. Rossi, P. Besmer, C.R. Antonescu, S. Zeng, R.P. DeMatteo
Administrative, technical, or material support: T.S. Kim
Study supervision: R.P. DeMatteo

NIH-PA Author Manuscript
NIH-PA Author Manuscript
NIH-PA Author Manuscript

NIH-PA Author Manuscript

NIH-PA Author Manuscript

NIH-PA Author Manuscript

improve the effects of imatinib. Instead, PLX3397 was a more potent KIT inhibitor than imatinib in vitro. PLX3397 therapy also induced substantial intratumoral fibrosis, which impaired the subsequent delivery of small molecules.

Conclusions—PLX3397 therapy has greater efficacy than imatinib in pre-clinical GIST models and warrants study in GIST patients. The resultant intratumoral fibrosis may represent one of the barriers to achieving complete tumor eradication.

Keywords

Gastrointestinal stromal tumor (GIST); imatinib; KIT; CSF1R; stroma

INTRODUCTION

GIST is the most common subtype of human sarcoma (1) and is a prototype of targeted molecular therapy in solid tumors. GIST is driven by an activating mutation in the *KIT* oncogene encoding the KIT receptor tyrosine kinase (2) or, less frequently, the *PDGFRA* oncogene encoding the related platelet-derived growth factor receptor alpha (PDGFRα) (3). Localized, primary GIST is treated with surgical resection, but historically up to 50% of patients developed tumor recurrence, after which median survival was less than 2 years (4). Molecular therapy has vastly improved the treatment of advanced GIST. Imatinib mesylate (Gleevec, Novartis) is a tyrosine kinase inhibitor that specifically targets oncogenic KIT and PDGFRα (5, 6) and benefits 80% of patients with advanced GIST (7). However, imatinib is rarely curative. Initially sensitive tumors acquire resistance at a median of only 18 months (8, 9), most often via a secondary *KIT* mutation (10). Sunitinib (Sutent, Pfizer) (11) and regorafenib (Stivarga, Bayer) (12) are 2 additional multi-kinase inhibitors that are approved by the Food and Drug Administration for patients who do not tolerate imatinib or whose tumors are imatinib-resistant. These drugs provide temporary benefit to some patients, but the overall median time to tumor progression is only 5–6 months (11, 12).

The limitations of available therapies underscore the need for more effective treatments in GIST. Approaches toward improving molecular therapy for cancers such as GIST include combination with other targeted inhibitors or conventional cytotoxic chemotherapy, alteration of the tumor microenvironment, and development of more potent molecular inhibitors. In a transgenic mouse model of GIST, Rossi *et al.* observed upregulation of Src family kinase signaling in response to imatinib and found modest histologic benefit from combining imatinib with dasatinib, a multi-kinase inhibitor that targets both KIT and Src (13). Focusing on the tumor microenvironment, we showed that GIST tumor cells suppressed anti-tumor $CD8^+$ T cell immunity via expression of indoleamine 2,3-dioxygenase (IDO) and that the T-cell activator anti-CTLA-4 was synergistic with imatinib (14).

PLX3397 (Plexxikon) is a novel, dual-specificity tyrosine kinase inhibitor that targets KIT and the related receptor tyrosine kinase colony-stimulating-factor-1 receptor (CSF1R, c-fms) with nanomolar potency (15, 16). CSF1R signaling is critical for macrophage survival and function, and tumor-associated macrophages (TAMs) are the most prevalent type of immune cell in human GIST (17). TAMs are thought to promote tumor growth through

NIH-PA Author Manuscript

NIH-PA Author Manuscript

NIH-PA Author Manuscript

immunosuppressive, angiogenic, and pro-metastatic effects (18). Recent animal studies have reported that PLX3397-mediated tumor macrophage depletion caused direct tumor regression (19) or improved response to chemotherapy (15, 16) or radiation therapy (20). Therefore, we sought to evaluate combined KIT and CSF1R inhibition in GIST. In a transgenic mouse model of GIST and in human GIST xenografts, we demonstrate superior anti-tumor efficacy of PLX3397 compared to imatinib. However, tumor response was associated with substantial intratumoral fibrosis that appeared to limit further drug delivery.

MATERIALS AND METHODS

Mice and treatments

Six to 15 week old *Kit*$^{V558del/+}$ mice (21) and C57BL/6J (B6) and NOD.Cg-*Prkdc*^{scid}*IL2rg*^{tm1Wjl}/SzJ (NSG) mice (Jackson Laboratory) were used. Mice were matched by age and sex. For xenograft experiments, 10^6 GIST-T1 cells in PBS were mixed 1:1 with growth factor reduced Matrigel (BD Biosciences) and injected subcutaneously into the right flank of NSG mice. Treatment was initiated at a mean tumor volume of 100 mm^3 as measured by the ellipsoid formula (1/2 × length × width × height). Imatinib (LC Laboratories) was administered in the drinking water at 600 mg/L. PLX3397 (15, 16) is a tyrosine kinase inhibitor that selectively inhibits KIT and CSF1R with biochemical half maximal inhibitory concentrations (IC_{50}) of 10 and 20 nM, respectively. PLX5622 (22) is a related compound with comparable potency against CSF1R (IC_{50} <10 nM), but 60-fold less potency against KIT. Both inhibitors were provided by Plexxikon and administered as formulated diet, 290 mg/kg chow (PLX3397), 1200 mg/kg chow (PLX5622), or control chow AIN-76A. Animals were maintained at Sloan-Kettering Institute, and procedures were approved by the Institutional Animal Care and Use Committee.

Flow cytometry

For tumor KIT^+ cell and macrophage analysis, tumors were minced, incubated in 12 mg/mL type 2 collagenase (Worthington Biochemical) plus 0.5 mg/mL DNAse I (Roche Diagnostics) for 30 minutes at 37°C, then washed through 100 then 40 μm nylon cell strainers (Falcon, BD Biosciences) with 1% fetal calf serum (FCS). For T cell analysis, tumors and draining lymph nodes (DLN) were mechanically dissociated as described (14). Spleens were mashed through a 70 μm strainer, incubated in ammonium chloride lysis buffer (eBioscience), quenched in 1% FCS, then washed through a 40 μm strainer. Bone marrow was flushed from one tibia per mouse, pooled by treatment group, homogenized by repeated aspiration through an 18-gauge needle, and then washed in 1% FCS. All cells were analyzed on a FACSAria (BD Biosciences) as described (14). Mouse-specific antibodies included CD45 (clone 30-F11), Kit (CD117) (2B8), CD11b (M1/70), CD3 (145-2C11), CD4 (GK1.5), Ly6C (AL-21), and Ly6G (1A8) from BD Biosciences; F4/80 (BM8) from Invitrogen; CD45 (30-F11), Kit (Ack2), CD8 (53–6.7), and FoxP3 (FJK-16s) from eBioscience. Intracellular staining for FoxP3 was performed using the FoxP3 Staining Buffer Set (eBioscience). Human-specific KIT antibody (YB5.B8) was purchased from BD Biosciences.

NIH-PA Author Manuscript

NIH-PA Author Manuscript

NIH-PA Author Manuscript

Histology

Mouse tumors were fixed in 4% paraformaldehyde, embedded in paraffin, and cut into 5 μm sections. Formalin-fixed, paraffin-embedded sections of surgical specimens were obtained from 17 GIST patients who consented to tissue analysis under an Institutional Review Board (IRB) protocol. Hematoxylin and eosin (H&E) and Masson's trichrome staining were performed using standard methods. Apoptosis was detected by terminal deoxynucleotidyl transferase-mediated dUTP nick end labeling (TUNEL) using the ApopTag Red In Situ Apoptosis Kit (Millipore) as directed. Slides were digitized using Mirax Scan (Zeiss). $TUNEL^+$ cells were counted as a percentage of total 4′,6-diamidino-2-phenylindole (DAPI) positive cells per high power field in 4–5 representative fields per tumor (Photoshop, Adobe). Staining for mouse type I collagen (Calbiochem rabbit polyclonal, 1:60, overnight at room temperature), and mouse/human KIT (citrate antigen retrieval, DAKO rabbit polyclonal, 1:600, overnight at 4°C) was performed as before (23). Slides were analyzed on an Axioplan2 wide-field microscope (Zeiss).

Western blot

Protein from frozen GIST tissue or GIST-T1 cells was analyzed as before (23). Antibodies against GAPDH and total and phosphorylated KIT (Tyr719), AKT (Ser473), S6 (Ser235/236), STAT3 (Ser727), and ERK1/2 (Thr202/Tyr204) were obtained from Cell Signaling Technology.

Peripheral blood analysis

Automated assessment of whole blood in EDTA was performed on an Idexx Procyte Dx® Hematology Analyzer (Idexx Laboratories). Manual white blood cell differential was performed on 100 cells on a blood smear stained with Accustain® Wright-Giemsa stain (Sigma-Aldrich).

In vitro assays

GIST-T1 cells have been described (24). HG129 cells were established under an IRB-approved protocol from an untreated primary gastric GIST harboring a *KIT* exon 11 mutation (45 bp insertion between phenylalanine 591 and glycine 592). GIST-T1 and HG129 cells were maintained in complete medium (RPMI with 10% FCS). NIH3T3 cells were provided by Dr. Jackie Bromberg and maintained in Dulbecco's Modified Eagle Medium with 10% FCS. To measure viability, GIST-T1 or HG129 cells were plated at 10^4 cells per well in a 96-well flat-bottomed plate (Falcon) and cultured for 72 hours at 37°C in complete medium with imatinib, PLX3397, or H_2O-or DMSO-only solvent control. Viability was then measured using the Cell Counting Kit-8 (Dojindo) as directed and normalized to control. IC_{50} values were calculated using nonlinear regression in Prism 5.0 (GraphPad Software). For protein analysis, GIST-T1 cells were plated at 2×10^6 cells per 100 × 20 mm cell culture dish (BD Biosciences) in serum-free medium overnight, then changed to serum-free medium containing either 10 or 40 nM of imatinib or PLX3397, or DMSO-only solvent control.

NIH-PA Author Manuscript
NIH-PA Author Manuscript
NIH-PA Author Manuscript

Collagen quantification

GIST-T1 or NIH3T3 cells were plated at 2×10^6 per 1 mL of complete medium per well in a 6-well plate (BD Biosciences) and cultured for 48 hours with 50 nM imatinib or PLX3397, or DMSO-only solvent control. Culture medium was then analyzed for soluble collagen content using the Soluble Collagen Assay (*Quick*Zyme BioSciences).

Cell isolation and RT-PCR

Bulk tumor cell suspensions were incubated with mouse CD45-specific immunomagnetic beads (Miltenyi Biotec), washed through a 40 μm strainer, centrifuged, and then run through a single LS column (Miltenyi) per 10^8 cells. $CD45^+$ cells were collected from the positive fraction. $CD45^-$ cells were incubated with mouse CD117 (Kit)-specific microbeads (Miltenyi), and then passed through 2 sequential LS columns for positive selection. Purity, assessed by flow cytometry, was greater than 95% ($CD45^-Kit^+$) and 85% ($CD45^+$). Total RNA from bulk tumor cell suspensions or $CD45^-Kit^+$ or $CD45^+$ cell fractions was isolated and analyzed by RT-PCR as before (23). Primers and TaqMan probes for mouse *Col1a1*, *Col1a2*, and *GAPDH* were obtained from Applied Biosystems. RT-PCR was performed using the ViiA 7 Real-Time PCR System (Applied Biosystems). Collagen mRNA expression was normalized to bulk tumor cell mRNA from control-treated mice.

Imaging and pharmacodelivery assays

Magnetic resonance imaging (MRI) was performed and analyzed as described (14). For tumor uptake and biodistribution studies, 100 μCi of ^{99m}Tc-Sestamibi (Nuclear Diagnostic Products) in 100 μL was administered via tail vein injection to $Kit^{V558del/+}$ mice that had been treated with control, imatinib, or PLX3397 for 2.5 weeks, then taken off treatment for 3 days. Radioactivity in the syringe before and after administration was measured in an energy-calibrated dose calibrator (CRC-15R; Capintec), and exact quantity received by each animal was determined. Mice were then sacrificed at 2 hours by CO_2 asphyxiation. Tissue was collected in pre-weighed tubes, weighed, and counted for radioactivity using a gamma counter (Perkin Elmer 1480 Wizard 3 Auto Gamma counter) with an auto-dynamic energy window near peak position 140 keV, which covered 90% of counts. The counts were then converted to activity (mCi) using a calibration factor, and percentage of injected dose per gram (%ID/g) was calculated by dividing by decay corrected injected activity and organ weight. For fluorescent tracer studies, $Kit^{V558del/+}$ mice were treated with control, imatinib, or PLX3397 for 10 weeks, then injected with a single intravenous (i.v.) dose of 15 mg/kg Hoechst 33342 dye (Molecular Probes, Invitrogen) or PBS control 50 minutes before sacrifice, followed by a single i.v. dose of 2 mg/kg fluorescein-conjugated *Lycopersicon esculentum* lectin (Vector Laboratories) or saline control 5 minutes before sacrifice. Tumors and spleens were embedded in Tissue-Tek O.C.T. Compound (Sakura) and cut into 5 μm thick cryosections. Slides were digitized as above, and 3 representative $0.6mm^2$ fields per tumor were analyzed in MetaMorph software (Molecular Devices). Average cellular Hoechst intensity was calculated with threshold area measurements and normalized to control-treated mice. Total lectin-staining vessel area per field was similarly calculated and normalized. Baseline autofluorescence was subtracted from each field analyzed.

NIH-PA Author Manuscript

NIH-PA Author Manuscript

NIH-PA Author Manuscript

Statistics

Data were analyzed using Prism 5.0. Unpaired two-tailed Student's *t* test or one-way ANOVA with Bonferroni post-test comparison was performed as applicable. When comparing tumor KIT^+ cell number between groups, cell counts were first log-transformed, and then analyzed by one-way ANOVA. A p-value < 0.05 was considered significant.

RESULTS

PLX3397 has greater anti-tumor effects than imatinib in *Kit*$^{V558del/+}$ mice

To investigate the efficacy of PLX3397 in GIST, we utilized transgenic *Kit*$^{V558del/+}$ mice, which spontaneously develop cecal GIST that is responsive to imatinib (14, 21, 25). Four weeks of PLX3397 reduced tumor weight and size to an even greater extent than imatinib (Fig. 1A–B). In addition, PLX3397 therapy resulted in 90% fewer Kit^+ tumor cells than imatinib (Fig. 1C) and a further decrease in tumor cell size and granularity, suggestive of apoptosis and necrosis (Fig. 1D). Histology confirmed the dramatic effects of PLX3397, as hypocellularity, necrosis, and fibrosis were more pronounced after PLX3397 therapy compared to imatinib (Fig. 1E). Consistent with our findings, PLX3397 also resulted in greater tumor apoptosis than imatinib (Fig. 1F). Overall, PLX3397 was more effective than imatinib in *Kit*$^{V558del/+}$ mice.

CSF1R inhibition does not account for the efficacy of PLX3397

PLX3397 and imatinib both inhibit Kit with nanomolar potency (15, 26). However, PLX3397 inhibits CSF1R more potently than imatinib (15, 26, 27), and CSF1R signaling contributes significantly to the maintenance and function of many types of macrophages, including tumor-associated macrophages (18). In *Kit*$^{V558del/+}$ mice, we found that PLX3397 depleted tumor macrophages to a much greater degree than imatinib (Fig. 2A), while less substantially affecting the frequency of other immune cells in the tumor, draining lymph node (DLN), and spleen (Supplemental Fig. S1A–B). We therefore hypothesized that increased CSF1R inhibition and greater tumor macrophage depletion accounted for the superior efficacy of PLX3397 in GIST. To test this, we combined imatinib with PLX5622 (22), a CSF1R-specific inhibitor of equal potency to PLX3397 that does not appreciably inhibit Kit. Despite comparable levels of tumor macrophage depletion as PLX3397 therapy (Fig. 2B), treatment with PLX5622 did not enhance the effect of imatinib on tumor weight, cell number, or histology, and PLX3397 remained the best therapy (Fig. 2C–E). These results suggested that tumor macrophage depletion was not responsible for the efficacy of PLX3397 in *Kit*$^{V558del/+}$ mice.

PLX3397 achieves greater KIT inhibition than imatinib in pre-clinical models of GIST

Aside from CSF1R, Kit is the only other kinase for which PLX3397 has a biochemical IC_{50} less than 100nM (15). Given the non-contributory effect of CSF1R inhibition on tumor size in vivo, we hypothesized that stronger Kit inhibition could explain the greater efficacy of PLX3397 compared with imatinib. In tumors from *Kit*$^{V558del/+}$ mice treated for 1 or 4 weeks, there was no significant difference in phospho-KIT to total KIT expression in PLX3397-treated tumors, at least in the residual tumor cells (Fig. 3A). However, PLX3397

NIH-PA Author Manuscript

NIH-PA Author Manuscript

NIH-PA Author Manuscript

reduced total Kit expression on a per cell basis more effectively than imatinib (Fig. 3B). Additionally, PLX3397 decreased tumor levels of phospho-Akt and the phospho-STAT3β isoform, both of which are downstream mediators of Kit signaling (Fig. 3A). PLX3397 did not reduce expression of the downstream mediator phospho-ERK1/2 (Fig. 3A), suggesting possible activation of compensatory signaling pathways, as has been demonstrated in other tumor models (28). Additional systemic manifestations of PLX3397-mediated Kit inhibition included hair depigmentation (Fig. 3C) and decreased erythropoiesis (Fig. 3D), two Kit-dependent processes that were not affected by a similar duration of treatment with imatinib. PLX3397 also decreased other hematopoietic lineages in the bone marrow to a greater extent than imatinib (Supplemental Fig. S1C), but was similar to imatinib in the degree of peripheral blood neutrophil and monocyte reduction (Fig. 3E–F). Collectively, these data suggested stronger inhibition of oncogenic as well as wild-type Kit during PLX3397 versus imatinib treatment in vivo.

To exclude potential pharmacokinetic differences between PLX3397 and imatinib, we compared the drugs in vitro against 2 human GIST cell lines that harbor an imatinib-sensitive, activating *KIT* exon 11 mutation similar to our $Kit^{V558del/+}$ mouse model. Indeed, PLX3397 decreased viability in both cell lines with two-fold greater potency than imatinib, with an IC_{50} of 8–18 nM versus 42 nM (Fig. 4A, $p<0.05$). At concentrations similar to the IC_{50} of each drug, i.e., 10 and 40 nM, PLX3397 also decreased phospho-KIT relative to total KIT more effectively than imatinib in vitro (Fig. 4B). Thus, PLX3397 was a stronger KIT inhibitor than imatinib in vitro. To translate these findings to an in vivo model of human GIST, we administered PLX3397 or imatinib to mice with established subcutaneous GIST-T1 xenografts. Analogous to our in vitro findings, PLX3397 reduced tumor size and KIT^{+} tumor cells more dramatically than imatinib (Fig. 4C–F). Although GIST-T1 cells contain a *KIT* exon 11 mutation and were sensitive to imatinib in vitro (Fig. 4A), imatinib was only cytostatic in vivo (Fig. 4C), as has been seen previously (29). In contrast, PLX3397 therapy caused substantial regression of GIST-T1 xenografts. Altogether, PLX3397 demonstrated greater anti-tumor efficacy than imatinib in murine and human GIST.

KIT-targeted therapies may be limited by stromal accumulation in GIST

While PLX3397 was clearly more effective than imatinib, our results raised the question of why PLX3397 could not achieve tumor eradication in our transgenic $Kit^{V558del/+}$ mouse model, where presumably there is relative tumor homogeneity. One possibility was that the stromal reaction we observed by H&E staining (Fig. 1E) was limiting further drug delivery to remaining tumor cells. To further analyze the stromal response to PLX3397 therapy, we examined tumors by Masson's trichrome staining, which stains collagen blue (Fig. 5A). By 1 week, PLX3397 substantially increased tumor collagen, and by 17 weeks, collagen accumulation was dramatic. Imatinib-treated tumors, on the other hand, accumulated collagen more slowly and to a lesser extent, and untreated tumors maintained only a constant, low level of collagen. Interestingly, human GISTs that were responsive to long-term imatinib therapy (e.g., 6 months) demonstrated comparable collagen staining to PLX3397-treated mouse tumors, whereas untreated human tumors or those that had acquired

NIH-PA Author Manuscript

NIH-PA Author Manuscript

NIH-PA Author Manuscript

resistance to imatinib did not (Fig. 5B). Therefore, the stromal reaction may not be specific to PLX3397 therapy.

Immunohistochemistry demonstrated the presence of fibrillar type I collagen within the stroma of PLX3397-treated tumors (Fig. 5C). Surprisingly, tumors were minimally infiltrated with fibroblast activation protein alpha (FAP)-expressing cells (not shown), which have been reported in other tumor models to represent activated cancer-associated fibroblasts, the major cellular source of collagen in epithelial-derived carcinomas (30). Instead, type I collagen transcripts were more highly expressed in Kit^{+} tumor cells than in other intratumoral cells after PLX3397 treatment (Fig. 5D). Furthermore, GIST cell lines produced soluble collagen in vitro, with a trend toward increased collagen in cells treated with imatinib or PLX3397 (Fig. 5E). Taken together, these findings suggested a final common pathway of tumor cell mediated collagen deposition and tissue remodeling caused by KIT inhibition in GIST.

Next, we assessed the viability of the residual tumor cells and adequacy of drug delivery. In $Kit^{V558del/+}$ mice treated with imatinib or PLX3397 for as long as 17 weeks, residual tumor cells maintained intact nuclei and Kit expression (Fig. 6A), similar to imatinib-responsive human GISTs (7, 31), suggesting viability despite chronic drug exposure. We proved in our $Kit^{V558del/+}$ mouse model that when PLX3397 was discontinued after 4 weeks of therapy, tumors re-grew over the next 11 weeks (Fig. 6B). To model drug delivery, we injected treated mice intravenously with the radioactive small molecule tracer ^{99m}Tc-sestamibi or the fluorescent DNA dye Hoechst 33342, both of which have similar molecular weight (approximately 780 and 620) to imatinib and PLX3397 (approximately 490 and 400). Indeed, there was markedly less tumor uptake of ^{99m}Tc-sestamibi in PLX3397-treated mice compared to control- or imatinib-treated mice (Fig. 6C, Supplemental Fig. S2). However, the ^{99m}Tc-sestamibi results only reflected average tracer uptake per gram of tumor, and not the relative amounts of intracellular versus extracellular matrix-bound tracer. To better assess drug delivery per tumor cell, we used Hoechst 33342. Consistent with our ^{99m}Tc-sestamibi findings, PLX3397 therapy markedly decreased tumor cell uptake of Hoechst dye compared to control or imatinib treatment (Fig. 6D). On the other hand, imatinib, and, to a lesser extent, PLX3397, increased tumor perfusion as estimated by lectin staining, compared with control. Overall, KIT inhibition induced tumor fibrosis in both murine and human GIST to a degree that was proportional to the potency or duration of KIT inhibition, and the resultant stromal accumulation appeared to impede small molecule delivery to residual tumor cells.

DISCUSSION

That molecular therapy rarely cures cancer is a major clinical problem and a driving force behind current oncologic research. Here, we demonstrate two unexpectedly related explanations for why KIT inhibition cannot completely eradicate GIST, despite the tumor's exquisite sensitivity to KIT inactivation, namely, suboptimal potency of currently available inhibitors and stromal impedance of drug delivery. Weinstein first introduced the theory of oncogene addiction to explain how the inactivation of a single driving oncogene can halt tumorigenesis despite the presence of numerous other genetic alterations (32). Studies in

NIH-PA Author Manuscript

NIH-PA Author Manuscript

NIH-PA Author Manuscript

conditional transgenic mouse models have indeed demonstrated that transcriptional or translational silencing of a single oncogene can cause complete regression of tumors as diverse as lymphoma (33), osteogenic sarcoma (34), and melanoma (35), through mechanisms including cell cycle arrest, apoptosis, differentiation, and senescence. Unfortunately, in GIST (9), as in other solid human tumors presumed to be oncogene-addicted, such as BRAF-mutated melanoma and epidermal growth factor receptor (EGFR)-mutated non-small cell lung cancer, pharmacologic inhibition has not been able to recapitulate the same degree of tumor regression. One of the simplest explanations for this discrepancy may be insufficient oncoprotein inhibition by currently available drugs. In the present study, we show that increased driver inhibition can cause even greater tumor regression than the first-line agent, imatinib, in both a transgenic mouse model of GIST and human GIST xenografts. The enhanced tumor cell eradication by PLX3397 depended on more potent KIT inhibition and not coincidental CSF1R-mediated macrophage depletion. The rapid kinetics of drug-induced apoptosis remain to be further investigated. Overall, our results reiterate the importance of driver inhibition in GIST and lend rationale to developing and testing more potent inhibitors, not only in GIST, but in other solid tumors with identified driver oncoproteins.

Notably, compared with imatinib, PLX3397 not only exhibited better anti-tumor efficacy, but also appeared to achieve greater systemic inhibition of wild type KIT in follicular melanocytes, which require KIT signaling for melanogenesis (36), and in a subset of hematopoietic stem cells, particularly erythroid precursors, which require KIT for normal red blood cell development (37). Depigmentation has been observed previously in mice (19) and humans (38) with PLX3397 but not imatinib. Such systemic manifestations reflect stronger KIT inhibition by PLX3397 but likely also signal the upper limit of the therapeutic index of KIT inhibition. Thus, although more potent KIT inhibitors could theoretically achieve even greater tumor responses than what we report here, such drugs would probably be limited by KIT-related toxicities such as bone marrow suppression. Notably, PLX3397 therapy did not predispose mice to increased infection. PLX3397 may therefore represent the most clinically attractive KIT inhibitor for GIST, achieving the highest level of KIT inactivation within an acceptable range of systemic toxicity.

From a broader perspective, the tumor microenvironment is gaining increasing recognition for its role in tumorigenesis and potential for therapeutic targeting. Relevant to the current study, resistance to molecular therapy can arise not only from mechanisms intrinsic to the tumor cell, but also from a variety of cell extrinsic mechanisms. Of particular concern in solid tumors is impaired drug delivery, which can result from abnormal tumor perfusion, increased tumor interstitial hydrostatic pressure, and extracellular matrix remodeling, all of which contribute to poor drug penetration into the tumor, sub-therapeutic drug levels within regions of the tumor, and ultimate treatment failure (39). Here, we demonstrate that potent KIT inhibition induces tumor fibrosis in a KIT-driven mouse model of GIST, with histologic changes reminiscent of the stromal accumulation observed in GIST patients responding to imatinib (31, 40). Importantly, we show that this fibrotic response is not just a correlate of tumor cell death, but potentially an obstacle to further small molecule delivery in treatment-responsive tumors. It was initially surprising that a KIT inhibitor as potent as PLX3397, for treatment durations as long as 1 month to greater than 1 year, could eradicate most but not

NIH-PA Author Manuscript

NIH-PA Author Manuscript

NIH-PA Author Manuscript

all tumor cells in our genetically homogeneous mouse model. Instead, residual tumor cells persisted, maintained the ability to resume growth off treatment, and retained drug sensitivity after re-growth (not shown). Such observations implicate reversible mechanisms of drug resistance, which could include cell-intrinsic mechanisms, such as drug-induced quiescence, or cell-extrinsic mechanisms, such as sub-therapeutic drug delivery. Using injected Hoechst dye to image tumor cell proximity to blood vessels in a subcutaneous lung carcinoma model, Chaplin *et al.* found that Hoechst-dim cells, which were multiple cell layers away from the nearest vessel, demonstrated less response than Hoechst-bright cells to a systemic injection of Adriamycin. These findings suggested that Hoechst fluorescence correlated with drug delivery and that delivery on a per cell basis affected drug efficacy (41). In the current study, we predicted that uniformly decreased Hoechst uptake in PLX3397- compared with control- or imatinib-treated tumors resulted from decreased tissue penetration due to extracellular matrix accumulation. The suspected impairment in drug delivery and tumor cell response is likely analogous to the results of Chaplin and colleagues. We acknowledge that our pharmacokinetic studies are limited by the use of small molecule tracers that are similar in molecular weight to our drugs of interest but obviously different in water and lipid solubility, molecular structure, and charge, all of which influence molecular flux through cells and tissue (39). Restricted by the lack of labeled drug forms that can be imaged with high enough resolution, we cannot directly measure imatinib or PLX3397 delivery to tumors on a per cell basis. However, we demonstrated the consistent finding of decreased small molecule uptake in PLX3397-treated tumors, regardless of chemical properties unique to ^{99m}Tc-sestamibi or Hoechst dye. Extrapolating our results to the agents under investigation, we propose that impaired drug penetration of treatment-responsive tumors may contribute to tyrosine kinase inhibitor resistance in GIST. Additional optimization of drug delivery will likely be necessary to maximize drug efficacy, and the rapid kinetics of PLX3397-mediated tumor fibrosis may serve as a useful model for future studies.

Elucidating the specific mechanisms of the fibrotic response to KIT inhibition may reveal new therapeutic targets in GIST. However, unlike most epithelial carcinomas, in which extracellular matrix derives from infiltrating fibroblasts (30), we have found that FAP$^+$ fibroblasts comprise only 1% of intratumoral cells in *Kit*$^{V558del/+}$ tumors (not shown). Functional studies of collagen production are ongoing in *Kit*$^{V558del/+}$ mice crossed to FAP-DTR mice, which express the diphtheria toxin receptor under the *FAP* promoter (42). However, we report here that GIST tumor cells themselves appear to be the most abundant source of collagen in the setting of KIT-targeted therapy. Thus, the very agents that ablate the majority of GIST tumor cells paradoxically induce a stromal response that may prevent complete tumor cell elimination. With no additional cell type to target, it may prove beneficial to modulate the stroma by either increasing degradation or inhibiting production of pathologic collagen. In a conditional transgenic mouse model of pancreatic adenocarcinoma, Provenzano *et al.* (43) and Jacobetz *et al.* (44) demonstrated that desmoplastic tumor stroma was rich in hyaluronic acid, a proteoglycan that in excess led to exceedingly high interstitial fluid pressures within the tumor, and that degradation of hyaluronic acid with systemically administered PEGylated hyaluronidase not only reduced tumor stroma but also improved chemotherapeutic delivery and response. Intratumoral

NIH-PA Author Manuscript

NIH-PA Author Manuscript

NIH-PA Author Manuscript

collagenase injection has similarly been reported to improve therapeutic delivery in various solid tumors (45), but it is impractical for the treatment of intra-abdominal tumors in the clinical setting, and a systemically administrable, non-toxic form of collagenase is not currently available. A trial of alternative anti-fibrotic agents, e.g., collagen synthesis inhibitors, warrants consideration in combination with KIT inhibition in GIST.

Although we hypothesized that collagen accumulation in PLX3397-treated tumors was in part due to the loss of macrophages, combined treatment with imatinib and macrophage depletion only resulted in mild tumor fibrosis. Therefore, despite the major physiologic role that macrophages play in homeostatic extracellular matrix degradation and remodeling, their loss in the setting of PLX3397 therapy did not appear to impact stromal accumulation. Such lack of effect suggests that the net state of extracellular matrix turnover in GIST depends more on the activity of the tumor cells, and less on traditionally implicated stromal cells such as macrophages and fibroblasts. That macrophage depletion did not impact overall tumor cell survival was also surprising and may highlight a limitation of our model, i.e., that $Kit^{V558del/+}$ murine GISTs do not metastasize or display tumor outgrowth in the setting of chronic therapy, two clinical problems in which depletion of tumor-promoting macrophages may actually improve outcome. Alternatively, sufficient oncoprotein inactivation may halt tumorigenesis to an extent that renders tumor immune responses less biologically relevant. A more aggressive GIST model is needed to investigate these questions.

We herein demonstrate that increased KIT inhibition translates into enhanced anti-tumor effects in clinically relevant mouse and xenograft models of GIST, but that such therapies may ultimately be limited by KIT-related systemic toxicities and, importantly, tumor cell-mediated fibrosis and probable impairment of drug delivery. Complete tumor eradication of non-operable GIST may require a combination of potent KIT inhibition, stromal modulators, and, perhaps in the setting of reduced fibrosis, immune activators. A potent KIT inhibitor such as PLX3397 may be most effective as first-line therapy in treatment-naïve tumors, which remain the most sensitive to oncogene inactivation and have likely acquired fewer genetic and non-genetic mechanisms of drug resistance. Sufficient tumor cell eradication up front may minimize the risk of residual cell persistence and later disease progression. Our results therefore have immediate applicability to the management of GIST patients and patients with similarly oncogene-addicted cancers.

Supplementary Material

Refer to Web version on PubMed Central for supplementary material.

Acknowledgments

Financial Support: The investigators were supported by U.S. National Institutes of Health (NIH) grants R01 CA102613 and T32 CA09501, the Geoffrey Beene Cancer Foundation, Mr. JHL Pit and Mrs. Pitvan Karnebeek and the Dutch GIST Foundation, the GIST Cancer Research Fund, Swim Across America, Stephanie and Fred Shuman through the Windmill Lane Foundation, and David and Monica Gorin (R.P.D.); F32 CA162721 and the Claude E. Welch Fellowship from the Massachusetts General Hospital (T.S.K.); and P50 CA140146 (P.B. and C.R.A.). The Molecular Cytology Core Facility was supported by Cancer Center Support Grant P30 CA008748. The content is solely the responsibility of the authors and does not necessarily represent the official views of the NCI or NIH.

NIH-PA Author Manuscript

NIH-PA Author Manuscript

NIH-PA Author Manuscript

We thank members of the Sloan-Kettering Institute Laboratory of Comparative Pathology, Molecular Cytology, Animal Imaging, Monoclonal Antibody, and Pathology core facilities, Colony Management Group, and Research Animal Resource Center. We thank Stephen Doty and the Analytical Microscopy Laboratory at Hospital for Special Surgery for insight and assistance with collagen staining, Mithat Gonen for assistance with statistical analysis, Gideon Bollag and Brian West of Plexxikon for providing the PLX3397 and PLX5622 compounds and related expertise, members of the laboratories of Peter Besmer, Cristina Antonescu, and Alan Houghton and Jedd Wolchok for helpful discussions and technical support, and Russell Holmes for administrative support.

References

1. Ducimetiere F, Lurkin A, Ranchere-Vince D, Decouvelaere AV, Peoc'h M, Istier L, et al. Incidence of sarcoma histotypes and molecular subtypes in a prospective epidemiological study with central pathology review and molecular testing. PloS One. 2011; 6:e20294. [PubMed: 21826194]
2. Hirota S, Isozaki K, Moriyama Y, Hashimoto K, Nishida T, Ishiguro S, et al. Gain-of-function mutations of c-kit in human gastrointestinal stromal tumors. Science. 1998; 279:577–80. [PubMed: 9438854]
3. Heinrich MC, Corless CL, Duensing A, McGreevey L, Chen CJ, Joseph N, et al. PDGFRA activating mutations in gastrointestinal stromal tumors. Science. 2003; 299:708–10. [PubMed: 12522257]
4. DeMatteo RP, Lewis JJ, Leung D, Mudan SS, Woodruff JM, Brennan MF. Two hundred gastrointestinal stromal tumors: recurrence patterns and prognostic factors for survival. Ann Surg. 2000; 231:51–8. [PubMed: 10636102]
5. Buchdunger E, Cioffi CL, Law N, Stover D, Ohno-Jones S, Druker BJ, et al. Abl protein-tyrosine kinase inhibitor STI571 inhibits in vitro signal transduction mediated by c-kit and platelet-derived growth factor receptors. J Pharmacol Exp Ther. 2000; 295:139–45. [PubMed: 10991971]
6. Heinrich MC, Griffith DJ, Druker BJ, Wait CL, Ott KA, Zigler AJ. Inhibition of c-kit receptor tyrosine kinase activity by STI 571, a selective tyrosine kinase inhibitor. Blood. 2000; 96:925–32. [PubMed: 10910906]
7. Demetri GD, von Mehren M, Blanke CD, Van den Abbeele AD, Eisenberg B, Roberts PJ, et al. Efficacy and safety of imatinib mesylate in advanced gastrointestinal stromal tumors. N Engl J Med. 2002; 347:472–80. [PubMed: 12181401]
8. Verweij J, Casali PG, Zalcberg J, LeCesne A, Reichardt P, Blay JY, et al. Progression-free survival in gastrointestinal stromal tumours with high-dose imatinib: randomised trial. Lancet. 2004; 364:1127–34. [PubMed: 15451219]
9. Blanke CD, Rankin C, Demetri GD, Ryan CW, von Mehren M, Benjamin RS, et al. Phase III randomized, intergroup trial assessing imatinib mesylate at two dose levels in patients with unresectable or metastatic gastrointestinal stromal tumors expressing the kit receptor tyrosine kinase: S0033. J Clin Oncol. 2008; 26:626–32. [PubMed: 18235122]
10. Antonescu CR, Besmer P, Guo T, Arkun K, Hom G, Koryotowski B, et al. Acquired resistance to imatinib in gastrointestinal stromal tumor occurs through secondary gene mutation. Clin Cancer Res. 2005; 11:4182–90. [PubMed: 15930355]
11. Demetri GD, van Oosterom AT, Garrett CR, Blackstein ME, Shah MH, Verweij J, et al. Efficacy and safety of sunitinib in patients with advanced gastrointestinal stromal tumour after failure of imatinib: a randomised controlled trial. Lancet. 2006; 368:1329–38. [PubMed: 17046465]
12. Demetri GD, Reichardt P, Kang YK, Blay JY, Rutkowski P, Gelderblom H, et al. Efficacy and safety of regorafenib for advanced gastrointestinal stromal tumours after failure of imatinib and sunitinib (GRID): an international, multicentre, randomised, placebo-controlled, phase 3 trial. Lancet. 2013; 381:295–302. [PubMed: 23177515]
13. Rossi F, Yozgat Y, de Stanchina E, Veach D, Clarkson B, Manova K, et al. Imatinib upregulates compensatory integrin signaling in a mouse model of gastrointestinal stromal tumor and is more effective when combined with dasatinib. Mol Cancer Res. 2010; 8:1271–83. [PubMed: 20736294]
14. Balachandran VP, Cavnar MJ, Zeng S, Bamboat ZM, Ocuin LM, Obaid H, et al. Imatinib potentiates antitumor T cell responses in gastrointestinal stromal tumor through the inhibition of Ido. Nat Med. 2011; 17:1094–100. [PubMed: 21873989]

NIH-PA Author Manuscript

NIH-PA Author Manuscript

NIH-PA Author Manuscript

15. DeNardo DG, Brennan DJ, Rexhepaj E, Ruffell B, Shiao SL, Madden SF, et al. Leukocyte complexity predicts breast cancer survival and functionally regulates response to chemotherapy. Cancer Discov. 2011; 1:54–67. [PubMed: 22039576]
16. Mitchem JB, Brennan DJ, Knolhoff BL, Belt BA, Zhu Y, Sanford DE, et al. Targeting tumor-infiltrating macrophages decreases tumor-initiating cells, relieves immunosuppression, and improves chemotherapeutic responses. Cancer Res. 2013; 73:1128–41. [PubMed: 23221383]
17. van Dongen M, Savage ND, Jordanova ES, Briaire-de Bruijn IH, Walburg KV, Ottenhoff TH, et al. Anti-inflammatory M2 type macrophages characterize metastasized and tyrosine kinase inhibitor-treated gastrointestinal stromal tumors. Int J Cancer. 2010; 127:899–909. [PubMed: 20013807]
18. Qian B, Pollard JW. Macrophage diversity enhances tumor progression and metastasis. Cell. 2010; 141:39–51. [PubMed: 20371344]
19. Prada CE, Jousma E, Rizvi TA, Wu J, Dunn RS, Mayes DA, et al. Neurofibroma-associated macrophages play roles in tumor growth and response to pharmacological inhibition. Acta Neuropathol. 2013; 125:159–68. [PubMed: 23099891]
20. Xu J, Escamilla J, Mok S, David J, Priceman S, West B, et al. CSF1R signaling blockade stanches tumor-infiltrating myeloid cells and improves the efficacy of radiotherapy in prostate cancer. Cancer Res. 2013; 73:2782–94. [PubMed: 23418320]
21. Sommer G, Agosti V, Ehlers I, Rossi F, Corbacioglu S, Farkas J, et al. Gastrointestinal stromal tumors in a mouse model by targeted mutation of the Kit receptor tyrosine kinase. Proc Natl Acad Sci U S A. 2003; 100:6706–11. [PubMed: 12754375]
22. Yu W, Chen J, Xiong Y, Pixley FJ, Yeung YG, Stanley ER. Macrophage proliferation is regulated through CSF-1 receptor tyrosines 544, 559, and 807. J Biol Chem. 2012; 287:13694–704. [PubMed: 22375015]
23. Zeng S, Feirt N, Goldstein M, Guarrera J, Ippagunta N, Ekong U, et al. Blockade of receptor for advanced glycation end product (RAGE) attenuates ischemia and reperfusion injury to the liver in mice. Hepatology. 2004; 39:422–32. [PubMed: 14767995]
24. Taguchi T, Sonobe H, Toyonaga S, Yamasaki I, Shuin T, Takano A, et al. Conventional and molecular cytogenetic characterization of a new human cell line, GIST-T1, established from gastrointestinal stromal tumor. Lab Invest. 2002; 82:663–5. [PubMed: 12004007]
25. Rossi F, Ehlers I, Agosti V, Socci ND, Viale A, Sommer G, et al. Oncogenic Kit signaling and therapeutic intervention in a mouse model of gastrointestinal stromal tumor. Proc Natl Acad Sci U S A. 2006; 103:12843–8. [PubMed: 16908864]
26. Deininger M, Buchdunger E, Druker BJ. The development of imatinib as a therapeutic agent for chronic myeloid leukemia. Blood. 2005; 105:2640–53. [PubMed: 15618470]
27. Dewar AL, Cambareri AC, Zannettino AC, Miller BL, Doherty KV, Hughes TP, et al. Macrophage colony-stimulating factor receptor c-fms is a novel target of imatinib. Blood. 2005; 105:3127–32. [PubMed: 15637141]
28. Logue JS, Morrison DK. Complexity in the signaling network: insights from the use of targeted inhibitors in cancer therapy. Genes Dev. 2012; 26:641–50. [PubMed: 22474259]
29. Gupta A, Roy S, Lazar AJ, Wang WL, McAuliffe JC, Reynoso D, et al. Autophagy inhibition and antimalarials promote cell death in gastrointestinal stromal tumor (GIST). Proc Natl Acad Sci U S A. 2010; 107:14333–8. [PubMed: 20660757]
30. Kalluri R, Zeisberg M. Fibroblasts in cancer. Nat Rev Cancer. 2006; 6:392–401. [PubMed: 16572188]
31. Joensuu H, Roberts PJ, Sarlomo-Rikala M, Andersson LC, Tervahartiala P, Tuveson D, et al. Effect of the tyrosine kinase inhibitor STI571 in a patient with a metastatic gastrointestinal stromal tumor. N Engl J Med. 2001; 344:1052–6. [PubMed: 11287975]
32. Weinstein IB. Cancer. Addiction to oncogenes--the Achilles heal of cancer. Science. 2002; 297:63–4. [PubMed: 12098689]
33. Felsher DW, Bishop JM. Reversible tumorigenesis by MYC in hematopoietic lineages. Mol Cell. 1999; 4:199–207. [PubMed: 10488335]
34. Jain M, Arvanitis C, Chu K, Dewey W, Leonhardt E, Trinh M, et al. Sustained loss of a neoplastic phenotype by brief inactivation of MYC. Science. 2002; 297:102–4. [PubMed: 12098700]

NIH-PA Author Manuscript

NIH-PA Author Manuscript

NIH-PA Author Manuscript

35. Hoeflich KP, Gray DC, Eby MT, Tien JY, Wong L, Bower J, et al. Oncogenic BRAF is required for tumor growth and maintenance in melanoma models. Cancer Res. 2006; 66:999–1006. [PubMed: 16424035]
36. Botchkareva NV, Khlgatian M, Longley BJ, Botchkarev VA, Gilchrest BA. SCF/c-kit signaling is required for cyclic regeneration of the hair pigmentation unit. FASEB J. 2001; 15:645–58. [PubMed: 11259383]
37. Nocka K, Majumder S, Chabot B, Ray P, Cervone M, Bernstein A, et al. Expression of c-kit gene products in known cellular targets of W mutations in normal and W mutant mice--evidence for an impaired c-kit kinase in mutant mice. Genes Dev. 1989; 3:816–26. [PubMed: 2473008]
38. Anthony SP, Puzanov I, Lin PS, Nolop KB, West B, Von Hoff DD. Pharmacodynamic activity demonstrated in phase I for PLX3397, a selective inhibitor of FMS and Kit. J Clin Oncol. 2011; 29(suppl):abstract 3093.
39. Minchinton AI, Tannock IF. Drug penetration in solid tumours. Nat Rev Cancer. 2006; 6:583–92. [PubMed: 16862189]
40. Agaram NP, Besmer P, Wong GC, Guo T, Socci ND, Maki RG, et al. Pathologic and molecular heterogeneity in imatinib-stable or imatinib-responsive gastrointestinal stromal tumors. Clin Cancer Res. 2007; 13:170–81. [PubMed: 17200352]
41. Chaplin DJ, Durand RE, Olive PL. Cell selection from a murine tumour using the fluorescent probe Hoechst 33342. Br J Cancer. 1985; 51:569–72. [PubMed: 2579667]
42. Kraman M, Bambrough PJ, Arnold JN, Roberts EW, Magiera L, Jones JO, et al. Suppression of antitumor immunity by stromal cells expressing fibroblast activation protein-alpha. Science. 2010; 330:827–30. [PubMed: 21051638]
43. Provenzano PP, Cuevas C, Chang AE, Goel VK, Von Hoff DD, Hingorani SR. Enzymatic targeting of the stroma ablates physical barriers to treatment of pancreatic ductal adenocarcinoma. Cancer Cell. 2012; 21:418–29. [PubMed: 22439937]
44. Jacobetz MA, Chan DS, Neesse A, Bapiro TE, Cook N, Frese KK, et al. Hyaluronan impairs vascular function and drug delivery in a mouse model of pancreatic cancer. Gut. 2013; 62:112–20. [PubMed: 22466618]
45. Netti PA, Berk DA, Swartz MA, Grodzinsky AJ, Jain RK. Role of extracellular matrix assembly in interstitial transport in solid tumors. Cancer Res. 2000; 60:2497–503. [PubMed: 10811131]

NIH-PA Author Manuscript

NIH-PA Author Manuscript

NIH-PA Author Manuscript

TRANSLATIONAL RELEVANCE

Targeted molecular therapies have revolutionized the treatment of patients with oncogene-addicted tumors such as GIST, but patients almost always develop drug resistance and disease progression. We demonstrated that PLX3397, a KIT and CSF1R inhibitor, achieved substantially more tumor regression than imatinib in both a transgenic mouse model of GIST and human GIST xenografts. PLX3397 therapy was also associated with greater systemic KIT inhibition, including bone marrow suppression, and induced severe intratumoral fibrosis, which appeared to impair further drug delivery. Our findings warrant the investigation of more potent KIT inhibitors in human GIST and identify the stromal response as a potential barrier to maximal drug delivery.

NIH-PA Author Manuscript
NIH-PA Author Manuscript
NIH-PA Author Manuscript

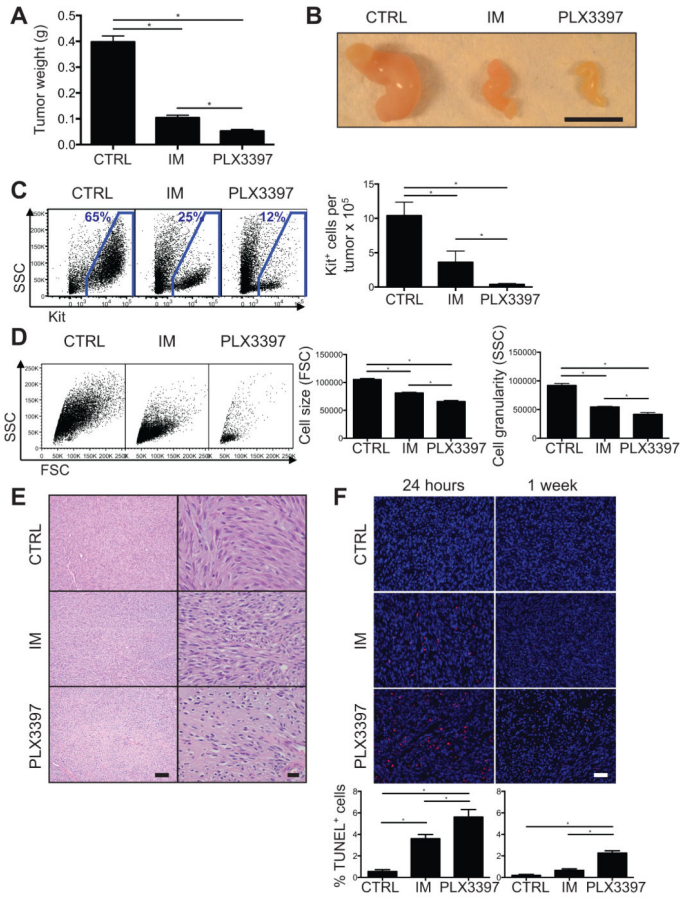

Figure 1. PLX3397 is superior to imatinib in *Kit*$^{V558del/+}$ mice

(A–E) Tumors from *Kit*$^{V558del/+}$ mice were analyzed following 4 weeks of treatment with regular drinking water and control chow (CTRL), imatinib in the drinking water and control chow (IM), or regular drinking water and PLX3397 chow (PLX3397). (A) Tumor weight. (B) Gross tumor appearance. Scale bar, 1 cm. (C–D) Tumors were digested with collagenase, and Kit$^+$ tumor cells were analyzed by flow cytometry. (C) Representative plots demonstrate Kit$^+$ tumor cells gated on CD45$^-$ cells (left). CD45$^-$Kit$^+$ cells quantified per tumor based on trypan blue exclusion and flow cytometry (right). (D) Representative plots gated on Kit$^+$ cells demonstrate forward and side scatter of light (FSC, SSC), which indicate cell size and granularity. (E) Tumor H&E staining. Scale bars, 100 (left) and 20 μm (right). (F) TUNEL staining of tumors from *Kit*$^{V558del/+}$ mice treated for either 24 hours or 1 week. Scale bar, 40 μm. TUNEL$^+$ cells, quantified as a percentage of total cells per high power field (below). Data in A, C are pooled from 4 experiments and in D–F are representative of 1–3 experiments, each with 2–6 mice per group. Bars show mean +/− SEM. *p<0.05.

NIH-PA Author Manuscript
NIH-PA Author Manuscript
NIH-PA Author Manuscript

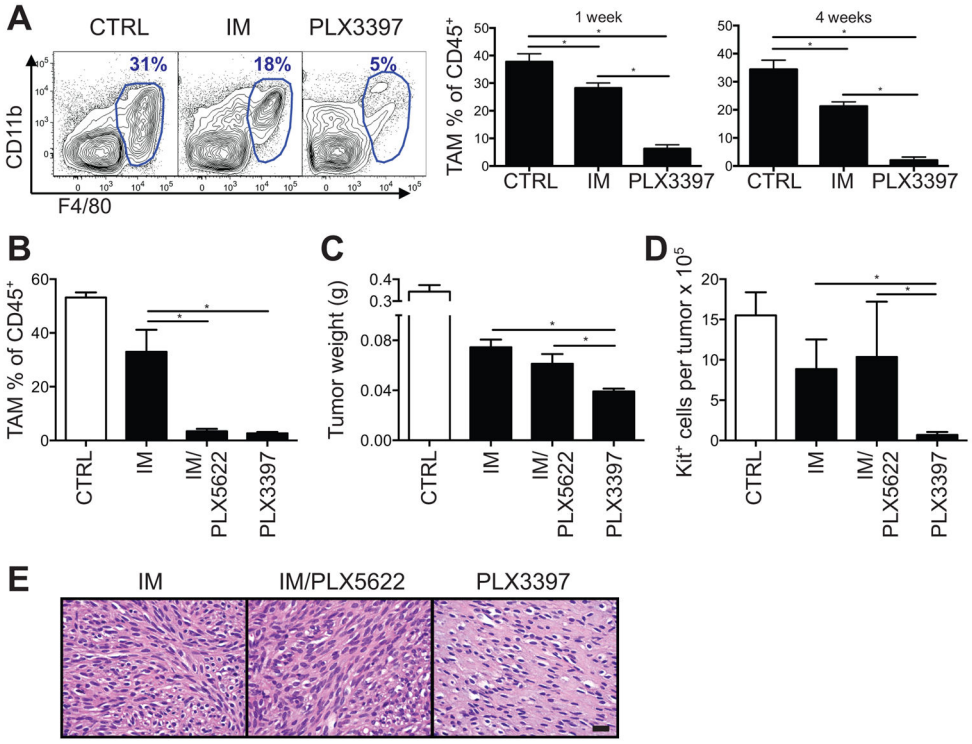

Figure 2. CSF1R inhibition does not account for PLX3397 effects

Kit$^{V558del/+}$ mice were treated for 4 weeks unless otherwise indicated. (A) Tumor-associated macrophages (TAMs, F4/80^{hi}) were measured by flow cytometry, with representative flow plots gated on CD45^{+} cells. (B) Tumor-associated macrophage depletion is shown as a percentage of CD45^{+} cells measured by flow cytometry. (C) Tumor weight. (D) Tumor Kit^{+} cell number, measured by trypan blue exclusion and flow cytometry. (E) Tumor H&E staining. Scale bar, 20 μm. Data in A, B, E are representative of 2–5 experiments and in C–D are pooled from 2 experiments, each with 2–5 mice per group. Bars show mean +/− SEM. *p<0.05.

NIH-PA Author Manuscript
NIH-PA Author Manuscript
NIH-PA Author Manuscript

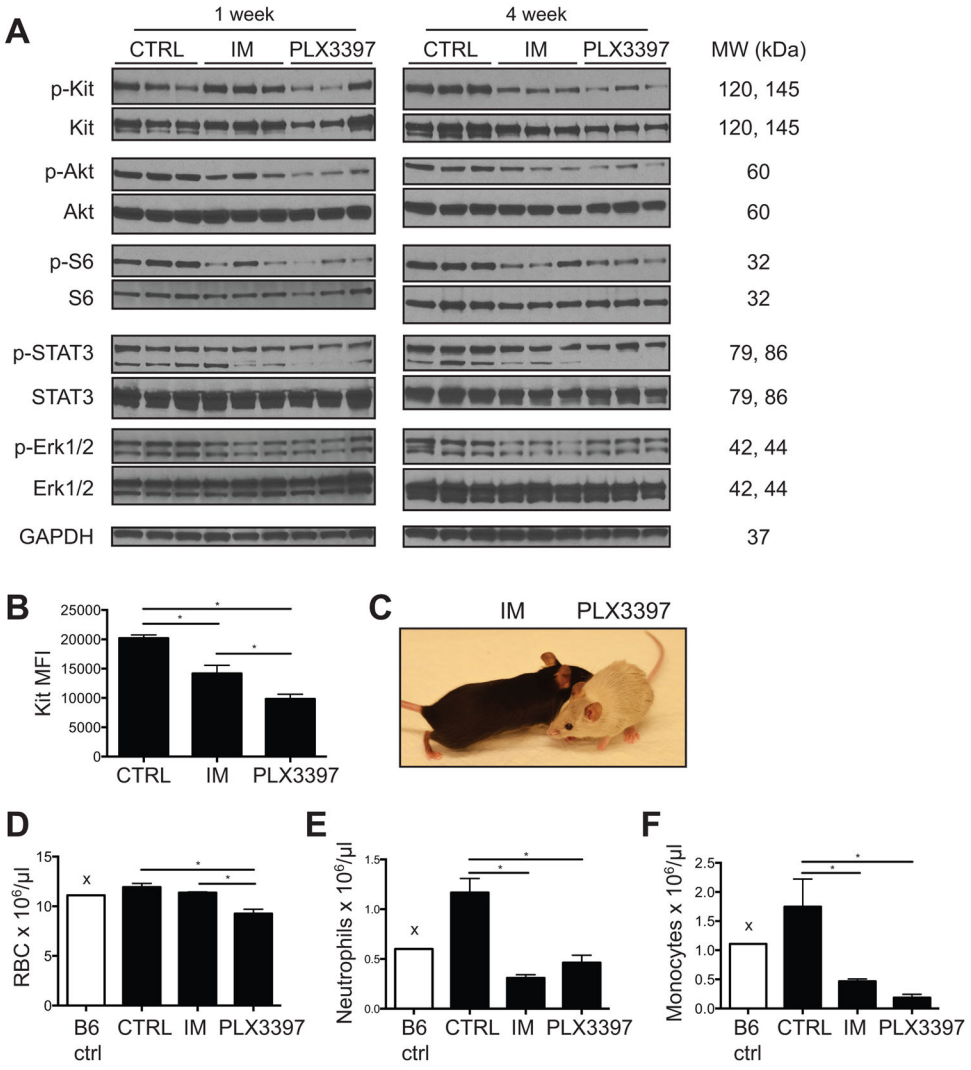

Figure 3. PLX3397 achieves stronger Kit inhibition than imatinib in vivo

(A) Western blot of tumors from *Kit*$^{V558del/+}$ mice treated as indicated. (B) Kit expression, shown as mean fluorescence intensity (MFI), was measured by flow cytometry of CD45^{-} Kit^{+} cells from tumors of *Kit*$^{V558del/+}$ mice treated for 4 weeks. (C) Representative photograph of *Kit*$^{V558del/+}$ mice treated with either imatinib or PLX3397 for 17 weeks. Peripheral red blood cells (RBC) (D), neutrophils (E), and monocytes (F) were quantified by automated complete blood count with manual white blood cell differential in *Kit*$^{V558del/+}$ mice treated for 4 weeks ("x" denotes single B6 control mouse). Data represent 3–6 mice per group and are shown as mean +/− SEM. *p<0.05.

NIH-PA Author Manuscript
NIH-PA Author Manuscript
NIH-PA Author Manuscript

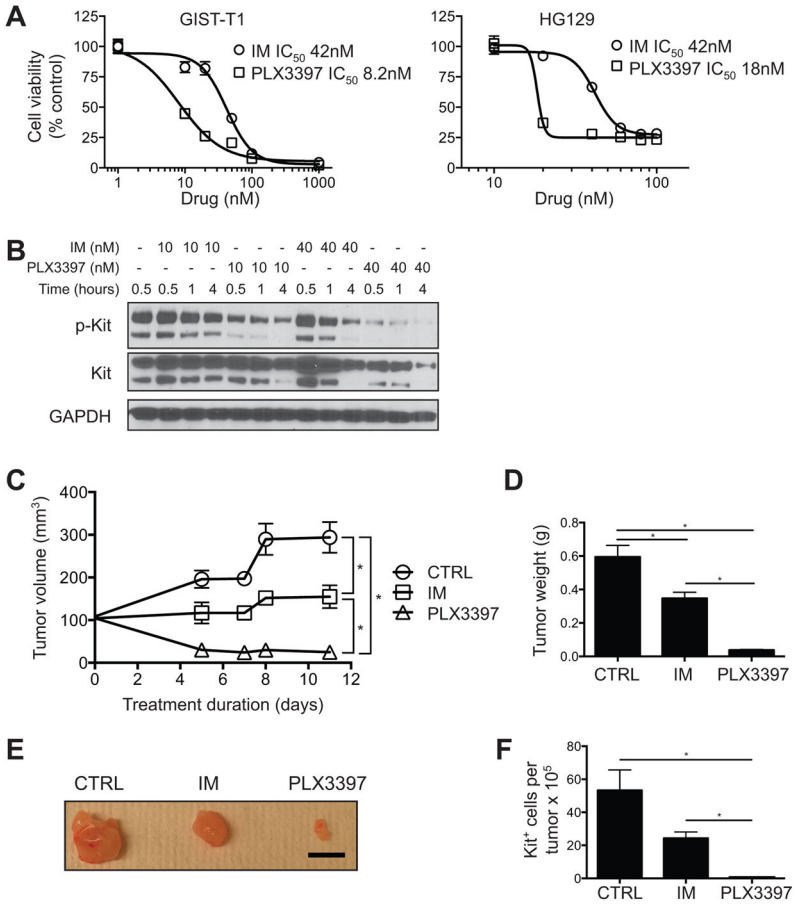

Figure 4. PLX3397 is more potent than imatinib against human GIST cell lines and xenografts

(A) Viability and IC_{50} in GIST-T1 and HG129 cells that were treated with imatinib or PLX3397 at the indicated concentrations. Curves represent nonlinear regression. (B) Western blot of GIST-T1 cells treated with imatinib or PLX3397. (C-F) NSG mice with established subcutaneous GIST-T1 xenograft tumors were treated for 11 days, after which tumors were analyzed. (C) Tumor volume. (D) Tumor weight. (E) Gross tumor appearance. Scale bar, 1 cm. (F) $CD45^{-}KIT^{+}$ tumor cell number as measured by trypan blue exclusion and flow cytometry. Data are representative of 1–6 experiments, each with 3–12 per group. Graphs show mean +/− SEM. *p<0.05.

NIH-PA Author Manuscript
NIH-PA Author Manuscript
NIH-PA Author Manuscript

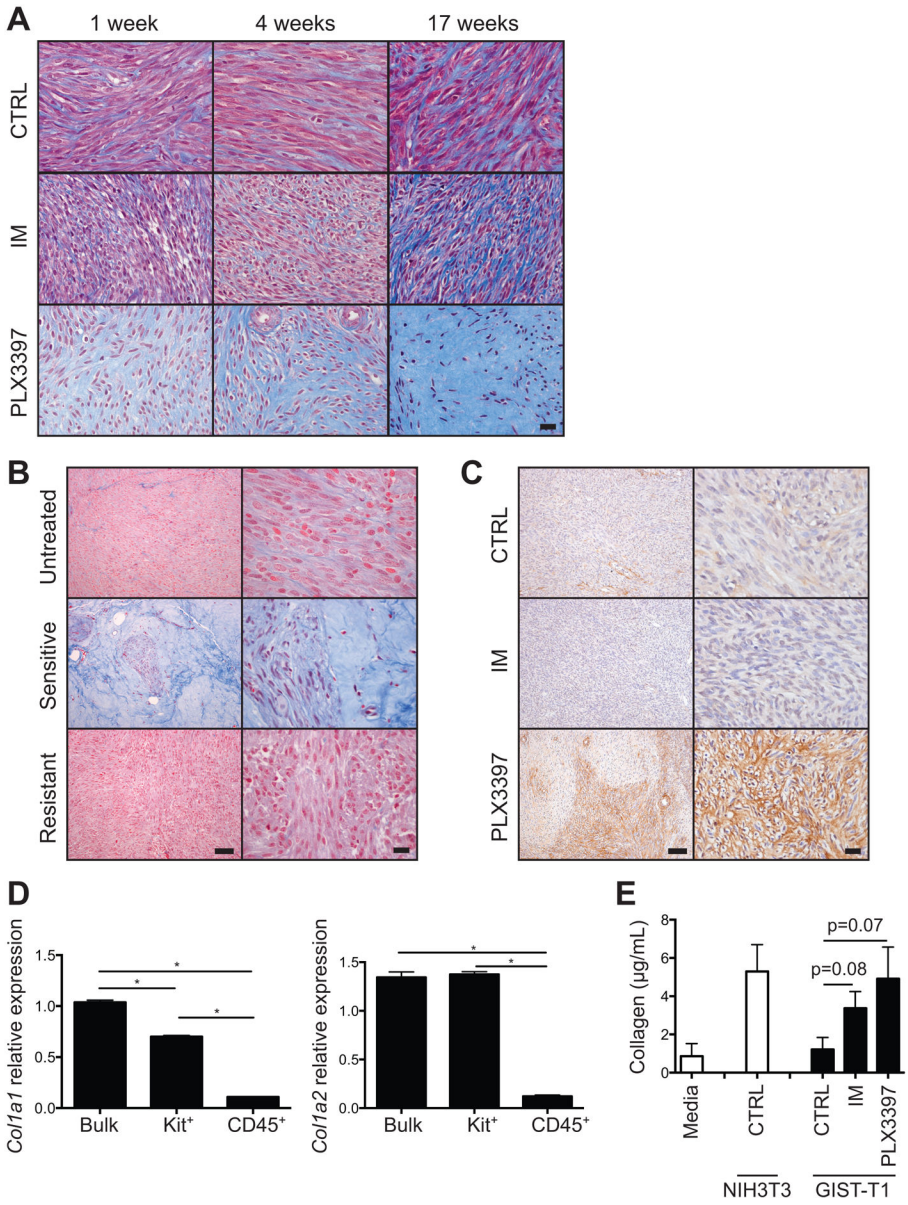

Figure 5. KIT inhibition induces tumor fibrosis proportional to magnitude of KIT inhibition

(A) Masson's trichrome staining of tumors from *Kit*$^{V558del/+}$ mice. Scale bar, 20 µm. (B) Masson's trichrome staining of human GIST specimens representative of 8 of 9 untreated, 5 of 6 imatinib-sensitive, and 2 of 2 imatinib-resistant patients. Scale bars, 100 (left) and 20 µm (right). (C) Type I collagen staining of tumors from *Kit*$^{V558del/+}$ mice treated for 4 weeks. Scale bars, 100 (left) and 20 µm (right). (D) *Col1a1* and *Col1a2* expression as measured by RT-PCR in bulk tumor, Kit^{+} tumor cells, or CD45^{+} stromal cells isolated by magnetic bead separation from tumors of *Kit*$^{V558del/+}$ mice treated with PLX3397 for 5 days. (E) Soluble collagen in conditioned media from GIST-T1 cells cultured for 48 hours as indicated. Mean of 5 replicates is shown. Collagen from cultured NIH3T3 fibroblasts is shown for comparison. The lower limit of detection was 3.5 µg/mL. Data are representative of 1–3 experiments, each with 2–8 per group. Bars show mean +/− SEM. *p<0.05.

NIH-PA Author Manuscript

NIH-PA Author Manuscript

NIH-PA Author Manuscript

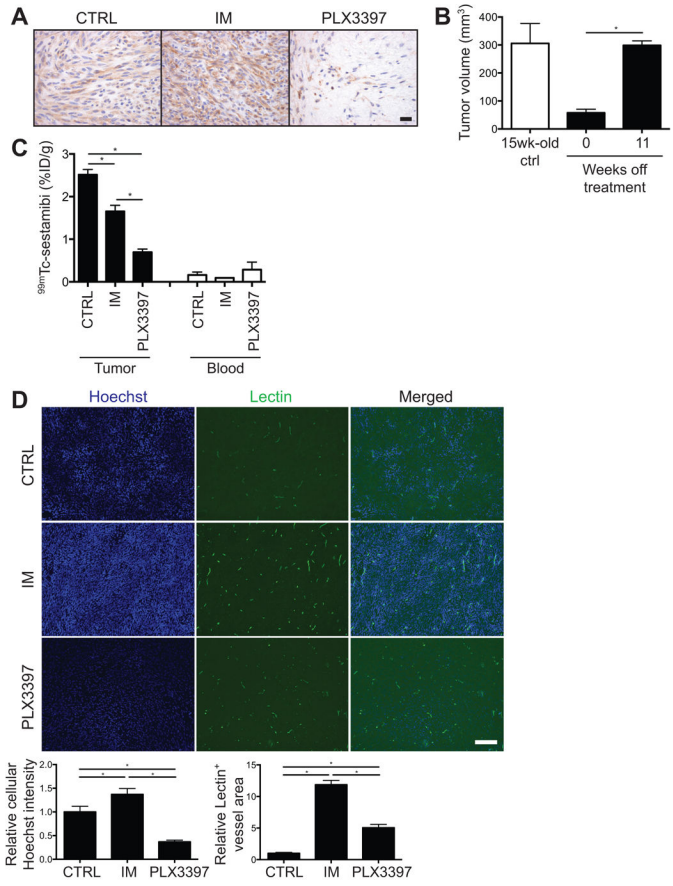

Figure 6. Tumor fibrosis impairs drug delivery in *Kit*$^{V558del/+}$ mice

(A) Kit staining of tumors from *Kit*$^{V558del/+}$ mice treated for 17 weeks. Scale bar, 20 μm. (B) *Kit*$^{V558del/+}$ mice were treated with PLX3397 for 4 weeks, then taken off treatment. Tumor volume was measured by MRI at 0 and 11 weeks off treatment and is shown in comparison to tumor volume in 15-week-old untreated control *Kit*$^{V558del/+}$ mice. (C) *Kit*$^{V558del/+}$ mice were treated for 2.5 weeks, followed by a single injection of ^{99m}Tc-sestamibi. Tumor and peripheral blood radioactivity is shown as a percentage of injected dose per gram (%ID/g). (D) Fluorescent microscopic images of tumors from *Kit*$^{V558del/+}$ mice treated for 10 weeks, followed by a single injection of Hoechst dye and fluorescein-conjugated lectin. Relative Hoechst intensity was measured on a per-cell basis. Scale bar, 500 μm. Quantification of average cellular Hoechst intensity and total lectin-positive area per representative field is shown normalized to control tumors. Data represent 2–5 mice per group. Bars show mean +/− SEM. *p<0.05.